

1  
2  
3  
4  
5  
6  
7  
8  
9  
10  
11  
12  
13  
14  
15  
16  
17  
18  
19  
20  
21  
22

**Supplementary Material**

**Colorimetric aptasensor for sensitive low-density lipoprotein**

**detection based on reduced oxide graphene@molybdenum disulfide–  
ferrocene nanosheets with peroxidase-like activity**

Guiyin Li<sup>1</sup>, Tingting Yu<sup>1,2</sup>, Haimei Li<sup>2</sup>, Bingbing Wan<sup>1,2</sup>, Xiaohong Tan<sup>1</sup>, Xueqing  
Zhou<sup>3\*</sup>, Jintao Liang<sup>2\*</sup>, Zhide Zhou<sup>2\*</sup>

1. College of Chemistry, Guangdong University of Petrochemical Technology,  
Guandu Road, Maoming, Guangdong 525000, People's Republic of China
2. School of Life and Environmental Sciences, Guilin University of Electronic  
Technology, Guilin, Guangxi 541004, People's Republic of China
3. Clinical Laboratory, the 924th Hospital of Chinese People's Liberation Army  
Joint Logistic Support Force, Guilin, Guangxi 541004, People's Republic of  
China

\*Corresponding author: zxqing181@163.com (X. Q. Zhou)

dxljt@guet.edu.cn (J. T. Liang)

zhouzhide10@guet.edu.cn (Z. D. Zhou)

Tel: +86-773-2305206; Fax: +86-773-2305206

## 1 1. Materials and Reagents

2 Graphene oxide (GO) was procured from Xianfeng NanoMaterials Technology  
3 Co., Ltd (Nanjing, China). Ascorbic acid (AA), N,N-Dimethylformamide (DMF),  
4 sodium hydroxide (NaOH), hydrogen peroxide (H<sub>2</sub>O<sub>2</sub>), glutaraldehyde (GA) were  
5 acquired from Xilong Scientific Co., Ltd. (Guangdong, China). Molybdenum  
6 disulfide (MoS<sub>2</sub>), N-Hydroxysuccinimide (NHS), sodium phosphate dibasic  
7 (Na<sub>2</sub>HPO<sub>4</sub>), sodium dihydrogen phosphate dehydrate (NaH<sub>2</sub>PO<sub>4</sub>), 3,3',5,5'-  
8 tetramethylbenzidine (TMB), bovine serum albumin (BSA), citric acid, sodium citrate  
9 were provided by Aladdin Reagent Co., Ltd. (Shanghai, China). Ferrocene-carboxylic  
10 acid (Fc), o-phenylene diamine (OPD) was acquired from Shanghai Macklin  
11 Biochemical Co., Ltd (Shanghai, China). β-mercaptoethylamine (β-ME) was from  
12 Changsha Nosebel Biotechnology Co., Ltd (Hunan, China). N-(3-  
13 Dimethylaminopropyl)-N'-ethylcarbodiimide hydrochloride (EDAC) was from Dalian  
14 Meilun Biotechnology Co., Ltd (Dalian, China). Terephthalic acid (PTA) was  
15 acquired from Bidepharm Scientific Co., Ltd (Shanghai, China). Immunoglobulin G  
16 (IgG), alpha-fetal protein (AFP), human serum albumin (HSA), horseradish  
17 peroxidase (HRP) was from Beijing Solarbio Science&Technology Co., Ltd (Beijing,  
18 China). Acetic acid was from Guangdong Guanghua Chemical Factory Co., Ltd  
19 (Guangdong, China). Sodium acetate was from Beijing Innochem  
20 Science&Technology Co., Ltd (Beijing, China). Low density lipoprotein (LDL), and  
21 high-density lipoprotein (HDL) was from Guangzhou Yiyuan Biotechnology Co., Ltd  
22 (Guangzhou, China). Cholesterol (chol), aminated LDL aptamer (LDLapt, 5'-NH<sub>2</sub>-  
23 ACCTCGATTTTATATTATTTTCGCTTACCAACAACACTGCAGA-3')[1],  
24 carboxyfluorescein modified LDLapt ((FAM)LDLapt, 5'-FAM-  
25 ACCTCGATTTTATATTATTTTCGCTTACCAACAACACTGCAGA-3'), Random

1 Sequence (Rand, 5'-NH<sub>2</sub>-TAA CGC TGA CGC TGA CCT TAG CTG CAT TTT  
2 ACA TGT TCC A-3') were got from Shenggong Bioengineering Co., Ltd (Shanghai,  
3 China). Clinical human serum samples were collected from the Guangxi Key  
4 Laboratory of Metabolic Disease Research of the 924th Hospital of the Chinese  
5 People's Liberation Army (Guilin, China). Ultrapure water (>18 MΩ) was used  
6 throughout. The stock solution of HAc-NaAc buffer, phosphate buffer solution (PBS)  
7 and citric acid/sodium citrate buffer solution were diluted for use by ultrapure water.  
8 All reagents were analytical grade and used directly.

## 9 **2. Apparatus**

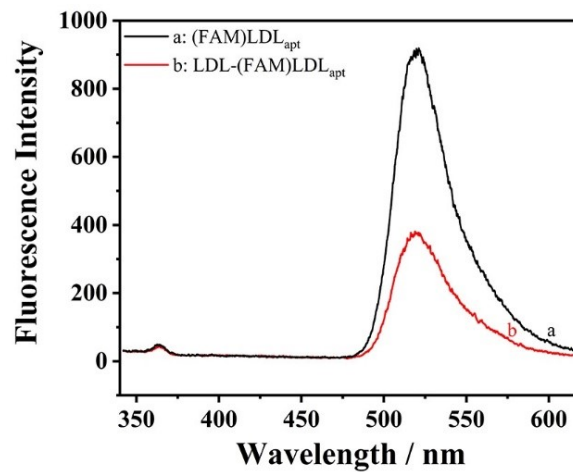
10 Transmission electron microscope (TEM) images and scanning electron  
11 microscopy (SEM) images were acquired using JEM-1200EX (JEOL, Japan)  
12 operating at an acceleration voltage of 100 kV and a Quanta 400 field environmental  
13 scanning electron microscope (FEI COMPANY, USA), respectively. Optical  
14 properties were determined using a Fourier-transform infrared spectroscopy (FT-IR,  
15 Nicolet-IS10, Nicolet, USA), UV-visible spectroscopy (UV-Vis, UH5300, HITACHI,  
16 Japan), a spectrofluorophotometer (F-4600, HITACHI, Japan), a Raman spectrometer  
17 (Raman, Renishaw, UK). X-ray photoelectron spectroscopy (XPS, ESCALAB 250xi,  
18 Thermofisher, USA) was used to analyze the elements of the nano-material. X-ray  
19 diffraction (XRD) images were from the GENESIS type energy spectrometer (EDAX,  
20 USA). Particle size potential was acquired from zeta sizer (ZS90, Melvin, UK). The  
21 conformational change of the secondary structure of protein was measured using the  
22 circular dichroism spectrum (CD, J-1500, Jasco, Japan).

## 23 **3. Specificity analysis between the LDLapt and LDL using fluorescence spectra**

24 100 μL of 1 μM (FAM)LDLapt was mixed with 100 μL of 1.0 μg/mL LDL, and  
25 incubated in the dark at 25°C for 1 h, then the above mixture and 200 μL of 0.5 μM

1 (FAM)LDLapt were detected by fluorescence spectrometer, respectively. The  
2 emission peak was set at 375 nm and the excitation peak at 520 nm.

3 Fig.S1 shows the fluorescence spectrum of (FAM)LDLapt. (FAM)LDLapt  
4 (curve a) emits fluorescence with an intensity of 919 due to its own fluorophores.  
5 After incubation of (FAM)LDLapt with LDL (curve b), the fluorescence intensity  
6 decreases to 379, indicating that the binding of (FAM)LDLapt with LDL led to  
7 changes in the structure of (FAM)LDLapt, thus leading to fluorescence quenching,  
8 which indicates that LDLapt is specific to LDL.



9

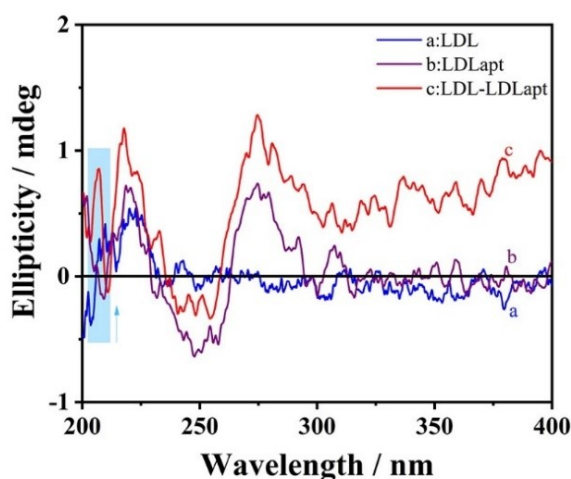
10 Fig.S1 Fluorescence spectrum of (FAM)LDLapt with or without LDL

#### 11 4. Specificity analysis of the LDLapt and LDL using circular dichroism

12 To study the conformational change of the secondary structure of the LDLapt  
13 upon the LDL, a CD analysis was conducted. 200  $\mu$ L of 2  $\mu$ M LDLapt was mixed  
14 with 200  $\mu$ L of 1.0  $\mu$ g/mL LDL, and incubated at 25°C for 1 h, then the above mixture,  
15 400  $\mu$ L of 1  $\mu$ M LDLapt, 400  $\mu$ L of 0.5  $\mu$ g/mL LDL were detected by CD,  
16 respectively. The range was 185 nm – 400 nm.

17 Fig.S2 shows the CD spectrum of LDLapt. LDL (curve a), as a class of  
18 lipoprotein, has a negative peak near 200 nm and a small but wide positive peak near  
19 220 nm, indicating that LDL is an irregular curly conformation. LDLapt (curve b) has

1 a positive peak near 200 nm, a weak negative peak near 208 nm, a strong positive  
 2 peak near 220 nm, a strong and wide negative peak near 250 nm, and a strong and  
 3 wide positive peak near 275 nm, showing a B-type right-handed double helix DNA  
 4 structure. After incubation of LDLapt with LDL (curve c), compared with the positive  
 5 peak of LDLapt and LDL, a new weak and narrow negative peak (region  $e\tau$ ) appears  
 6 in LDL-LDLapt between 210.4 nm – 211.4 nm. Moreover, compared with the  
 7 negative peak of LDLapt and LDL, a new strong but narrow positive peak (region  $\&$ )  
 8 appears in LDL-LDLapt between 232.7 nm – 235.8 nm, indicating that the  
 9 conformation of LDLapt is changed after LDLapt is bound to LDL, and LDLapt is  
 10 specific to LDL.



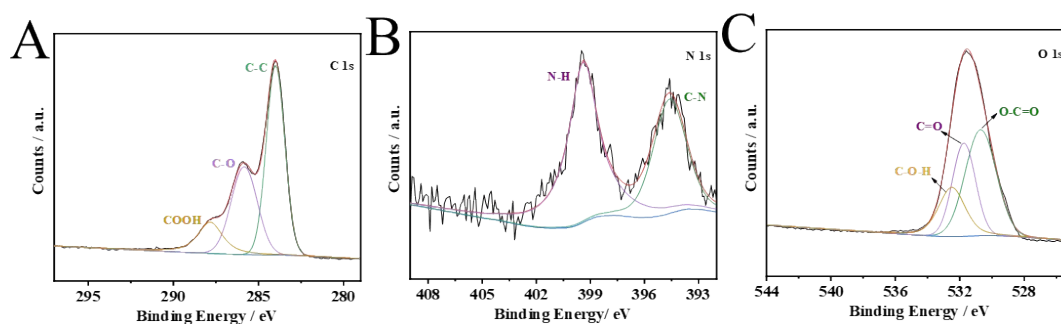
11

12 Fig.S2 Circular dichroism analysis of LDLapt with or without LDL

### 13 5. XPS analysis of C, N, O of rGO@MoS<sub>2</sub>-Fc

14 Fig.S3 is the XPS analysis of C, N, O of rGO@MoS<sub>2</sub>-Fc. FigS3A shows the XPS  
 15 energy spectrum analysis of C 1s with binding energies of 284 eV, 285.8 eV, 287.8  
 16 eV for C-C, C-O, and COOH functional groups, respectively. Fig.S3B shows the XPS  
 17 energy spectrum analysis of N 1s, and the C-N at 394.6 eV and the N-H bond at 399.4  
 18 eV indicate the presence of amino groups on MoS<sub>2</sub> and the formation of MoS<sub>2</sub>-Fc  
 19 with Fc through amide bonding. Fig.S3C shows the XPS spectra of O 1s with binding

1 energies of 530.7 eV, 531.7 eV, and 532.5 eV for O-C=O, C=O, and C-O-H  
2 functional groups, respectively. XPS spectra of C 1s and O 1s indicate the presence of  
3 rGO or Fc in the prepared rGO@MoS<sub>2</sub>-Fc.



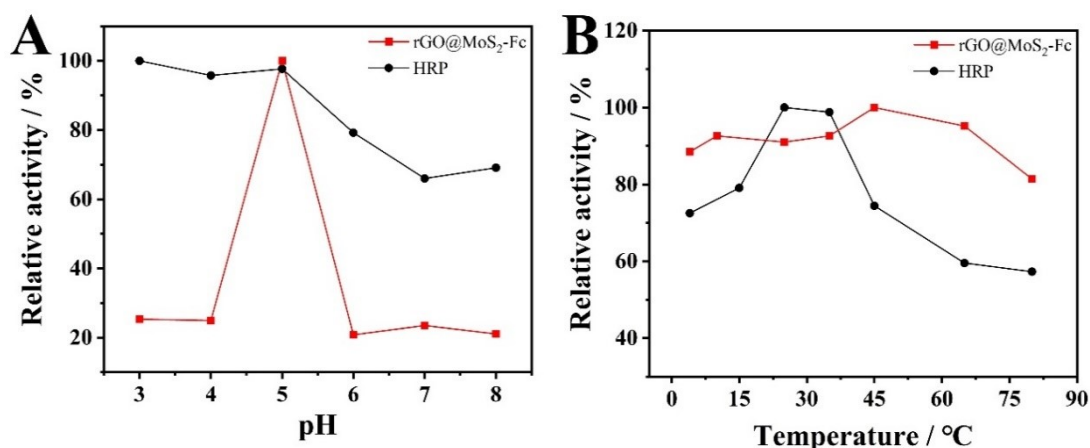
4  
5 Fig.S3 (A) XPS spectra of C 1s., (B) XPS spectra of N 1s, and (C) XPS spectra of O  
6  
7 1s of rGO@MoS<sub>2</sub>-Fc

## 7 6. Stability of rGO@MoS<sub>2</sub>-Fc and HRP

8 The pH stability and temperature stability of rGO@MoS<sub>2</sub>-Fc were measured  
9 under the same experimental conditions as well as that of HRP, and the two were  
10 compared. rGO@MoS<sub>2</sub>-Fc or HRP, OPD-H<sub>2</sub>O<sub>2</sub> solution, different pH (3.0 - 8.0) of  
11 PBS (125 mM) were incubated in the dark at room temperature for 1 h, then  
12 transferred for UV-Vis spectrophotometry to observe the absorbance evolution at 420  
13 nm. The temperature stability of rGO@MoS<sub>2</sub>-Fc was measured as well as that of HRP,  
14 and the two were compared. rGO@MoS<sub>2</sub>-Fc or HRP, OPD-H<sub>2</sub>O<sub>2</sub> solution, phosphate  
15 buffer (PBS, 125 mM, pH 5.0) were incubated in the dark at different room  
16 temperature (4°C - 80°C) for 1 h, then transferred for UV-Vis spectrophotometry to  
17 observe the absorbance evolution at 420 nm.

18 Fig.S4A shows the pH stability of rGO@MoS<sub>2</sub>-Fc and HRP. The catalytic  
19 activity of HRP is more stable between pH 3.0 - pH 8.0 and decreases with increasing  
20 pH, finally remaining above 60%, while the catalytic activity of the rGO@MoS<sub>2</sub>-Fc is  
21 best at pH 5.0, and decreases to 20% at other pH values. Fig.S4B shows the

1 temperature stability of rGO@MoS<sub>2</sub>-Fc and HRP. The catalytic activity of HRP  
2 decreases to less than 80% at low and high temperature, while the catalytic activity of  
3 rGO@MoS<sub>2</sub>-Fc nanozyme remained above 80% between 4°C and 80°C, indicating  
4 that rGO@MoS<sub>2</sub>-Fc has good temperature stability.



5  
6 Fig.S4 (A) The pH stability and (B) temperature stability of rGO@MoS<sub>2</sub>-Fc and HRP,  
7 respectively.

### 8 7. Study on the enzymatic catalytic activity of rGO@MoS<sub>2</sub>-Fc over time

9 The enzymatic catalytic activity of rGO@MoS<sub>2</sub>-Fc over time in HAc-NaAc  
10 buffer was studied. 10.0 μL of 50 mM OPD, 10.0 μL of 100 mM H<sub>2</sub>O<sub>2</sub>, and 20.0 μL  
11 of 1 mg/mL rGO@MoS<sub>2</sub>-Fc were added into 60.0 μL HAc-NaAc buffer (125 mM, pH  
12 5.5). The mixture was incubated in the dark at room temperature, and then the  
13 absorption curve was measured by UV-Vis every 5 minutes.

14 Fig.S5 shows the UV-Vis spectra of rGO@MoS<sub>2</sub>-Fc in HAc-NaAc buffer over  
15 time (0 - 30 min). As shown in Fig.S5, the absorbance of rGO@MoS<sub>2</sub>-Fc increases  
16 with time in 25 min, especially, the absorbance of rGO@MoS<sub>2</sub>-Fc does not change  
17 after 30 min, thus, 25 min is regarded as the optimal reaction time of rGO@MoS<sub>2</sub>-Fc  
18 in HAc-NaAc buffer.

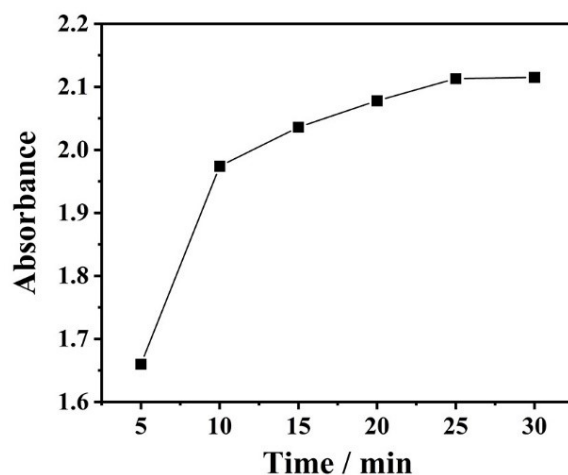


Fig.S5 UV-Vis spectra of rGO@MoS<sub>2</sub>-Fc over time

1

2

### 3 **8. Optimization of experimental conditions for the LDL colorimetric** 4 **aptasensor**

5

As shown in Fig.S6A, the absorbance values increased when the LDLapt  
6 concentration increased from 0.5  $\mu$ M to 1  $\mu$ M, and gradually decreased when the  
7 concentration increased from 1  $\mu$ M to 6  $\mu$ M, indicating that when the LDLapt  
8 concentration was 1  $\mu$ M, the LDL captured by the constructed colorimetric aptamer  
9 sensor and the amount of bound rGO@MoS<sub>2</sub>-Fc/LDLapt could make the most  
10 chromogenic substrate. Changes in the concentration of LDLapt affect the amount of  
11 LDL captured, which in turn affects the amount of rGO@MoS<sub>2</sub>-Fc/LDLapt bound,  
12 resulting in differences in color or absorbance. Choosing the optimal concentration of  
13 LDLapt can specifically bind more LDL, and then construct more rGO@MoS<sub>2</sub>-  
14 Fc/LDLapt/LDL/LDLapt systems, and improve the selectivity and sensitivity of the  
15 sensor. Therefore, 1.0  $\mu$ M LDLapt concentration was chosen as the optimal  
16 experimental condition.

17 The change of LDL incubation time affects the amount of LDL captured, and  
18 insufficient time will lead to the inability of LDLapt to bind to LDL. In order to  
19 ensure the full combination of LDLapt and LDL, it is often necessary to set a long

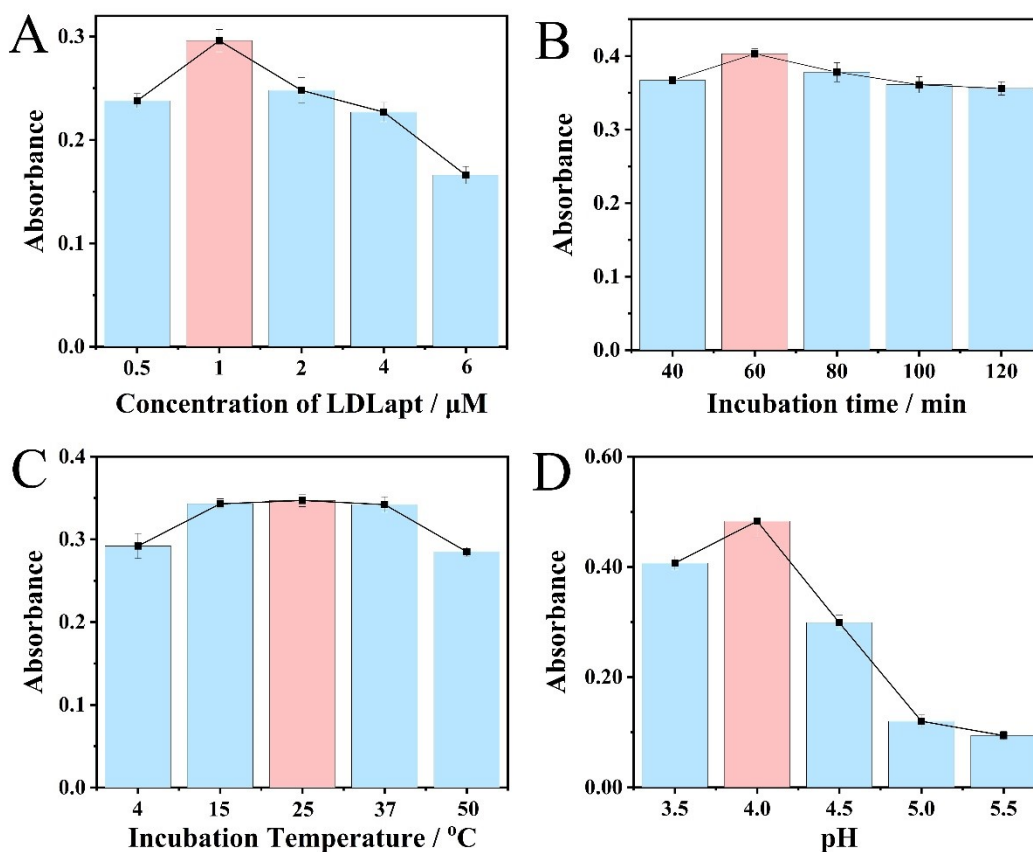


1 enough reaction time. Therefore, finding the best LDL incubation time can make the  
2 detection of the sensor faster. As shown in Fig.S6B, when the incubation time of LDL  
3 was increased from 40 min to 60 min, the absorbance value increased, while when the  
4 incubation time was increased from 60 min to 120 min, the absorbance value  
5 gradually decreased and there was no significant change between the current values,  
6 indicating that the constructed colorimetric aptamer sensor was sufficient to capture  
7 LDL and bind to it when the incubation time of LDL was 60 min, so 60 min was  
8 chosen as the optimal incubation time for LDL.

9 The change of LDL incubation temperature will reduce the activity of LDL or  
10 make it denatured and inactivated, so that the concentration of LDL can not be  
11 accurately detected or even detected. Therefore, the reaction at the most appropriate  
12 temperature can ensure the accuracy of the sensor in detecting LDL concentration. As  
13 shown in Fig.S6C, when the incubation temperature of LDL increased from 4°C to  
14 25°C, the absorbance value increased, and when the incubation temperature increased  
15 from 25°C to 50°C, the absorbance value gradually decreased, and the number of  
16 bound LDL and rGO@MoS<sub>2</sub>-Fc/LDLapt decreased due to the denaturation and  
17 inactivation of LDL at 50°C, indicating that the best sensor effect was achieved when  
18 the incubation temperature of LDL was 25°C. Therefore, 25°C LDL incubation  
19 temperature was chosen as the optimal experimental condition.

20 Because the change of the pH value of HAc-NaAc buffer solution affects the pH  
21 value of the whole solution reaction system, and then affects the catalytic  
22 performance of rGO@MoS<sub>2</sub>-Fc, which makes it unable to rapidly and completely  
23 catalyze the decomposition of H<sub>2</sub>O<sub>2</sub> to produce ·OH. Therefore, it is necessary to  
24 choose the best buffer solution pH to ensure the sensitivity of sensor detection. As  
25 shown in Fig.S6D, when the pH of HAc-NaAc buffer solution increased from 3.5 to

1 4.0, the absorbance value increased; and when it increased from 4.0 to 5.5, the  
 2 absorbance value gradually decreased, indicating that the best sensor effect was  
 3 achieved when the pH was 4.0, which is easier to catalyze the decomposition of  $H_2O_2$   
 4 to produce  $\cdot OH$ , so pH 4.0 was chosen as the optimal experimental condition  
 5 Therefore, pH 4.0 was chosen as the optimal experimental condition.



6  
 7 Fig.S6 Optimization of experimental conditions. (A) Concentration of LDLapt. (B)  
 8 Incubation time. (C) Incubation temperature. (D) pH of HAc-NaAc buffer

### 9 9. Cost-benefit analysis of rGO@MoS<sub>2</sub>-Fc colorimetric aptamer sensor

10 In the process of material preparation, the cost of GO and other materials and  
 11 reagents used in each synthesis is about 1.15 yuan. In the construction of sensor  
 12 system, the cost of using LDLapt is about 6.21 yuan each time, and the cost of using  
 13 materials and reagents such as OPD is about 0.1 yuan each time.

1 The main instruments used for testing are ultraviolet-visible spectrophotometer,  
2 model UH5300, HITACHI, Japan. The price is about 20.00 w~40.00 w.

### 3 **References**

4 [1] D. Klapak, S. Broadfoot, G. Penner, A. Singh, E. Inapuri, PLOS ONE, 2018, 13,  
5 1-16. <https://doi.org/10.1371/journal.pone.0205460>.